Early science with the Large Millimeter Telescope: molecules in the extreme outflow of a protoplanetary nebula

A. I. Gómez-Ruiz,[1]⋆ L. Guzman-Ramirez,[2,3] E. O. Serrano,[4] D. Sánchez-Argüelles,[4] A. Luna,[4] F. P. Schloerb,[5] G. Narayanan,[5] M. S. Yun,[5] R. Sahai,[6] A. A. Zijlstra,[7] M. Chavez-Dagostino,[4] A. Montaña,[1] D. H. Hughes[4] and M. Rodríguez[4]

[1]*CONACYT–Instituto Nacional de Astrofísica, Óptica y Electrónica, Luis E. Erro 1, 72840 Tonantzintla, Puebla, México*
[2]*European Southern Observatory, Alonso de Córdova 3107, Casilla 19001, Santiago, Chile*
[3]*Leiden Observatory, Leiden University, Niels Bohrweg 2, NL-2333 CA Leiden, the Netherlands*
[4]*Instituto Nacional de Astrofísica, Óptica y Electrónica, Luis E. Erro 1, 72840 Tonantzintla, Puebla, México*
[5]*Department of Astronomy, University of Massachusetts, Amherst, MA 01003, USA*
[6]*Jet Propulsion Laboratory, MS 183-900, California Institute of Technology, Pasadena, CA 91109, USA*
[7]*Jodrell Bank Centre for Astrophysics, School of Physics and Astronomy, University of Manchester, Manchester M13 9PL*

ABSTRACT

Extremely high velocity emission, likely related to jets, is known to occur in some protoplanetary nebulae. However, the molecular complexity of this kinematic component is largely unknown. We observed the known extreme outflow from the protoplanetary nebula IRAS 16342−3814, a prototype water fountain, over the full frequency range from 73–111 GHz with the Redshift Search Receiver (RSR) on the Large Millimetre Telescope. We detected the molecules SiO, HCN, SO and ^{13}CO. All molecular transitions, with the exception of the latter, are detected for the first time in this source and all present emission with velocities up to a few hundred km s^{-1}. IRAS 16342−3814 is therefore the only source of this kind presenting extreme outflow activity in all these molecules simultaneously, with SO and SiO emission showing the highest velocities found for these species in protoplanetary nebulae. A tentative weak SO component with a full width at half-maximum of ∼700 km s^{-1} remains to be confirmed. The extreme outflow gas consists of dense gas ($n_{H_2} > 10^{4.8}$–$10^{5.7}$ cm^{-3}) with a mass larger than ∼ 0.02–0.15 M$_\odot$. The relatively high abundances of SiO and SO may be an indication of oxygen-rich extremely high velocity gas.

Key words: stars: late-type – ISM: abundances – ISM: molecules.

1 INTRODUCTION

One of the mysteries of planetary nebulae (PNe) is the morphological changes that transform the spherical circumstellar envelopes (CSEs) of asymptotic giant branch (AGB) stars into highly bipolar/multipolar PNe. To understand the mechanism of such changes, the short transition phase in between should be explored. At some point in the late AGB stage, a process (or processes) accelerates and imposes bipolarity upon the slow, spherical AGB winds. Key questions that remain to be answered are what produces bipolarity in these objects and at what stage bipolarity manifests itself.

It has been suggested that fast collimated outflows and jets, active during the protoplanetary nebula (pPN) and/or very late AGB phase, are responsible for the drastic change in the mass-loss geometry and dynamics of the system in transition (Sahai & Trauger 1998). Among the outflows observed in pPNe, there is a category that stands out because of its peculiar kinematics. Sahai & Patel (2015)

coined the term 'extreme outflow' to define those pPNe with molecular outflows showing line emission in excess of ∼100 km s^{-1}, with a few examples identified by these authors and a few others found in the literature fulfilling this definition. Such spectral features in pPN outflows may be the equivalent of the so-called extremely high velocity (EHV) emission observed in protostellar outflows, which is thought to be an unambiguous jet signature (Bachiller 1996). Indeed, some studies in pPN outflows support this similarity (see e.g. Balick et al. 2013). Star-formation outflows presenting this peculiar spectral feature have been used as the perfect tool to study the kinematics of the different components of the outflow process, but in particular allowing a more complete study of the jet (EHV) component, otherwise contaminated by the other outflow components, such as the cavity and the bow shocks (see e.g. Lefloch et al. 2015). The identification of extreme outflows from pPNe is therefore relevant, since their study has the potential to put constraints on theoretical models that include jets.

Water-fountain pPNe are a particularly interesting subclass of pPNe, the original distinguishing characteristic of which is the

⋆ E-mail: aigomez@inaoep.mx

presence of very high-velocity red- and blueshifted H_2O and OH maser features. The velocity separations of the water fountains can be as high as $500 \, \text{km s}^{-1}$ (Gómez et al. 2011). This velocity spread of the masers may suggest a relation between water fountains and the extreme outflows traced by thermal molecular lines (Yung et al. 2016). IRAS 16342−3814 is the nearest (∼2 kpc: Sahai et al. 1999) and best-studied water fountain. Its morphology has been resolved in the optical, near-infrared and mid-infrared. Radio observations show water masers spread over a wide range of radial velocities ($>100 \, \text{km s}^{-1}$: Chong, Imai & Diamond 2015). CO (2–1) and CO (3–2) observations reveal a massive, high-velocity molecular outflow (He et al. 2008; Imai et al. 2009, 2012). The CO line profiles exhibit both a narrow component with an expansion velocity of $40 \, \text{km s}^{-1}$ and wide wings with an expansion velocity of $100 \, \text{km s}^{-1}$ (Imai et al. 2012).

The molecular complexity of pPNe with outflows is well-known (e.g. Sanchez Contreras, Bujarrabal & Alcolea 1997); however, in most cases the molecular emission cannot be related unambiguously to the jet component. Water fountains, on the other hand, have been poorly covered by molecular line observations. The EHV emission from pPN outflows has been little explored in molecular species other than CO. Recent studies in star-formation outflows with EHV emission have unveiled a velocity-dependent shock chemistry and a peculiar composition of the EHV gas (Tafalla et al. 2010). With this background, we started a project to study the molecular composition of pPN outflows with known EHV emission from CO lines. In this Letter, we present wide-band observations towards the pPN IRAS 16342−3814, with the double aim of providing a molecular census in this prototype water fountain and studying the molecular composition of the EHV gas.

2 OBSERVATIONS

Using the Large Millimetre Telescope Alfonso Serrano (LMT) in its early science phase, we observed the known EHV outflow pPN IRAS 16342−3814 with the Redshift Search Receiver (RSR). Observations were performed on 2016 March 19 and 24, with a sky opacity, $\tau_{225 \, \text{GHz}}$, ranging from 0.16–0.20 and an instrumental T_{sys} from 109–116 K. Observations were centred on the coordinates RA (J2000) = $16^h37^m39^s.91$, Dec. (J2000) = $−38°20'17''.3$, with the OFF beam 39 arcsec apart. Pointing accuracy was found to be better than 2 arcsec. The total ON time integration was 1.5 h.

The RSR is an autocorrelator spectrometer that covers the frequency range 73–111 GHz at 31-MHz spectral resolution, which corresponds to ∼$100 \, \text{km s}^{-1}$ at 90 GHz (Erickson et al. 2007). In its early science phase, the LMT operates with a 32-m active surface, which then results in a half-power beam width (HPBW) ∼26 arcsec at the centre of the band (RSR data have been reported in a number of articles: for an example see Cybulski et al. 2016). Autocorrelations, spectra co-adding, calibration and baseline removal were carried out with the Data REduction and Analysis Methods in PYTHON (DREAMPY) software. A careful inspection of each scan shows reasonably flat baselines and therefore only a linear fit in DREAMPY was used to remove the baseline to each 5-min spectrum. However, the average 90-min spectrum showed a subtle low-frequency continuous wave signal along the full RSR band. In deep ($\sigma < 1$ mK) RSR spectra, the atmosphere fluctuations have a non-negligible contribution to the baseline, which is reflected into a structured noise spanning each board. We then constructed a template for this structured signal using a third-order Savitsky–Golay filter with a window size of 1 GHz, which is significantly greater than the width of the lines in our spectrum (see section 3). Our approach is slightly
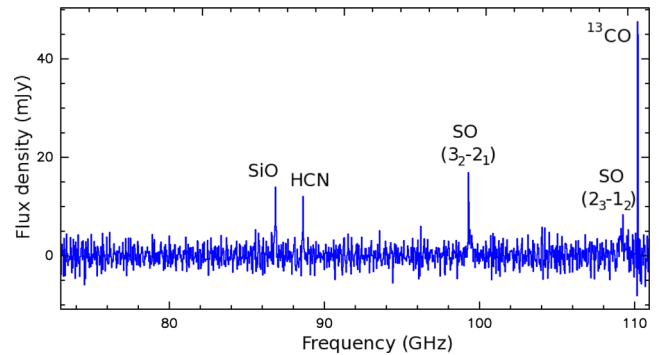

Figure 1. LMT/RSR observations of the pPN IRAS 16342−3814. We present the full bandwidth covered by RSR. The species identified are SiO, HCN, SO and ^{13}CO.

different from the technique used in Cybulski et al. (2016), since we calculate and subtract the template for each individual spectrum rather than applying the filter for the final spectrum only. Atmospheric residuals can be very different from scan to scan, therefore our final average spectrum is less affected by artefact signals produced by subtraction effects, which may be produced only if the final spectrum is passed through the filter. The filtered spectrum has an average root-mean-square (r.m.s.) noise of 0.29 mK. Note, however, that the noise is not uniform along the band and some parts are less noisy. To convert antenna temperature units (T_A^*) to Jy, we used a conversion factor (Jy K^{-1}) of 6.4 for $\nu < 92$ GHz and 7.6 for $\nu > 92$ GHz. Finally, for consistency, the line parameters were obtained from a spectrum re-sampled to the worse spectral resolution corresponding to the lowest frequency transition detected (SiO 2–1; i.e. $108 \, \text{km s}^{-1}$).

3 RESULTS

In Fig. 1, we present the 3-mm spectrum of IRAS 16342−3814. The frequency displayed is topocentric; however, the difference with respect to the rest frame is much smaller than a channel width and therefore equal to rest frequency within the uncertainties. Table 1 summarizes the molecular lines detected and their parameters. The following five molecular transitions were detected: SiO (2–1), HCN (1–0), SO (3_2–2_1), SO (2_3–1_2) and ^{13}CO (1–0). All but ^{13}CO are first detections in this source. All these lines can be fitted by Gaussian profiles centred close to the systemic velocity (within the uncertainties). Fig. 2 shows the SiO (2–1), HCN (1–0) and ^{13}CO (1–0) lines with their respective Gaussian fits. In the case of SO (3_2–2_1), a two-component Gaussian fit seems to be needed to account for the emission (see below). In peak intensity, the strongest line is ^{13}CO (1–0), while the weakest is SO (2_3–1_2). SiO (2–1) and HCN (1–0) are approximately similar in peak intensity. Regarding the line width, SiO (2–1) is about 40 per cent wider (full width at half-maximum (FWHM) of $322\pm47 \, \text{km s}^{-1}$) than HCN (1–0), while the narrowest lines are SO (2_3–1_2) and ^{13}CO (1–0), with FWHM between 108 and $120 \, \text{km s}^{-1}$.

In Fig. 3, we show Gaussian fits to the SO (3_2–2_1) and SO (2_3–1_2) profiles. In a first attempt, we tried to fit a single Gaussian component to the SO (3_2–2_1) line profile (black line in the upper panel of Fig. 3). The resulting FWHM is $241\pm42 \, \text{km s}^{-1}$. However, we notice a substantial residual coming from the blueshifted part of the spectrum. Such a residual may suggest the presence of a very fast blueshifted wing, with a maximum radial velocity (above a 3σ level) of ∼ $−700 \, \text{km s}^{-1}$. A two-component Gaussian fit reduces

Table 1. Molecular lines detected in IRAS 16342−3814 with the LMT/RSR and their parameters.[a]

Transition	Frequency (GHz)	HPBW ($''$)	E_u (K)	Line peak (mJy)	V_{peak} (km s^{-1})	FWHM (km s^{-1})	$\int S\,dv$ (mJy km s^{-1})
SiO (2–1)	86.847	27.1	6.2	10.4	−5(8)	332(47)	3677(427)
HCN (1–0)	88.623	26.6	12.8	10.3	−7(18)	276(58)	3023(460)
SO (3_2–2_1)	99.296	23.8	9.2	15.6	+3(12)	239(39)	3988(453)
SO (2_3–1_2)	109.252	21.6	21.1	10.3	+17(11)	108(61)	1217(395)
^{13}CO (1–0)	110.201	21.4	5.3	66.8	+2(7)	120(20)	8572(359)

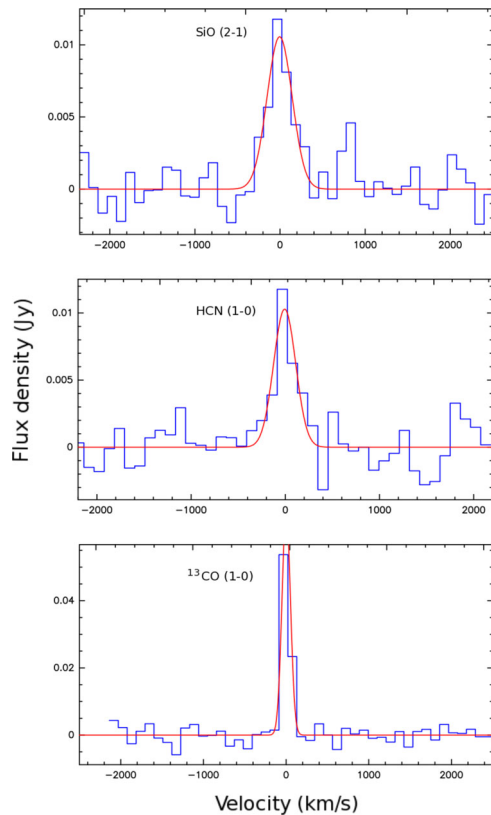*Note.* [a]Line parameters from Gaussian fits; errors indicated in brackets.

Figure 2. Line profiles of the molecules SiO (2–1), HCN (1–0) and ^{13}CO (1–0); all have been fitted with a one-component Gaussian. The velocity axis is with respect to the local standard of rest (LSR) and the spectral resolution is 108 km s^{-1}. Using the Gaussian fits, we measure the line width: SiO and HCN have FWHM > 200 km s^{-1}, while the ^{13}CO line has a FWHM of 120 km s^{-1}.

Figure 3. Spectra of the SO lines detected towards the pPN IRAS 16342−3814 and Gaussian fits to their profiles (red line). The velocity axis is with respect to LSR and the spectral resolution is 108 km s^{-1}. The upper panel shows two different fits: a black one using only one Gaussian fit and a red fit using two Gaussian components. The two-fit component shows a component in the SO (3_2–2_1) line with a FWHM of >600 km s^{-1}, centred at negative velocities, suggesting an extremely fast blueshifted outflow. For the lower panel, we only fitted a narrow component to the SO (2_3–1_2) line with a FWHM of ∼108 km s^{-1}.

the residual by a factor of 3 (red line in the upper panel of Fig. 3), resulting in a narrow component at the systemic velocity with a FWHM of 139±74 km s^{-1} and a wide component with a FWHM of 748±157 km s^{-1} shifted to negative velocities (peak velocity −315±100 km s^{-1}). In the search for other contaminants that may broaden the SO (3_2–2_1) line, we checked for line transitions inside the range of frequencies that fall into the same range of line emission (defined within a 3σ level). The HCCNC ($J = 10$–9) line lies at 99.40 GHz; however, this molecule is more common in C-rich objects and IRAS 16342−3814, on the other hand, is an O-rich object (as proven by the simultaneous detection of SO and SiO), suggesting such an identification to be unlikely. Furthermore, the frequency of the HCCNC line falls at the high-frequency edge of the broad component. The implications of the wide component are important, since this would represent the highest velocity ever observed in a molecular outflow of a pPN. Although the careful reduction we have performed gives confidence that such a feature is real, given
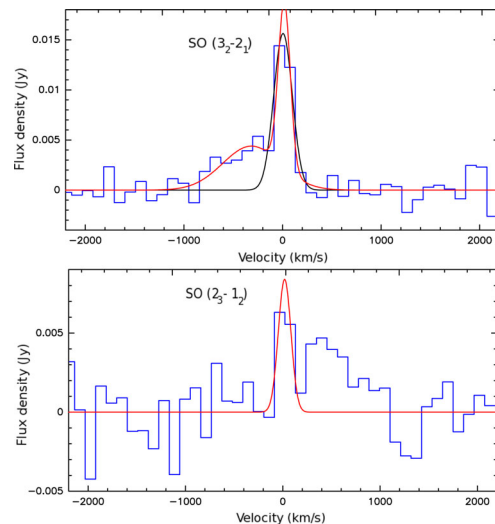
its weakness we prefer to be cautious and defer the confirmation of this feature to future deeper observations (unfortunately no further observations of this object could be taken during the early science season). The SO (2_3–1_2) line is detected at ∼4σ in only one channel (note, however, a feature at ∼ +400 km s^{-1} that we ignore because it barely reaches ∼3σ and is located in the noisiest part of the band), hence only one Gaussian component is required to fit the emission. This component has a FWHM of 108±61 km s^{-1} and is centred at the systemic velocity.

4 DISCUSSION

4.1 Molecular composition and physical properties

Before our observations, molecular line data of IRAS 16342−3814 revealed the presence of a fast bipolar outflow and a slowly expanding torus/CSE (Imai et al. 2012). The CO outflow has a FWHM ∼150 km s^{-1} (Imai et al. 2009), while the H$_2$O masers show a total velocity spread of 270 km s^{-1}, with their proper motions indicating three-dimensional velocities of approximately ±180 km s^{-1} (Claussen, Sahai & Morris 2009). Our observations show the HCN (1–0) emission with a FWHM similar to the velocity spread of the H$_2$O masers, while the SO emission shows slightly lower values. On the other hand, the SiO emission seems to present higher velocities

Table 2. Molecular abundances and column densities.

Molecule	N (cm^{-2})	X^a
SiO	1.4E17	5.2E-7
HCN	2.7E16	9.6E-8
SO	7.0E16	4.0E-7
^{13}CO	5.6E18	2.0E-5^b

Notes. $^a X = X(^{13}\mathrm{CO}) \times N/N(^{13}\mathrm{CO})$.
^{b}Bujarrabal et al. (2001).

than the water masers. The ^{13}CO (1–0) FWHM is similar to the ^{12}CO measurements.

OH 231.8+4.2 is the other pPN showing high-velocity SO emission with a line width $\sim$100 km s^{-1} (with a notably asymmetric profile: Claude, Avery & Matthews 2000). Therefore, our detection is the highest velocity SO emission found in a pPN. HCN has been detected at extreme velocities only in CRL 618, with a total velocity range similar to our source ($\sim$250 km s^{-1}: Sánchez Contreras & Sahai 2004). SiO emission, on the other hand, has been previously detected at extreme velocities of $\leq$150 km s^{-1} only in IRAS 08005$-$2356 (albeit in the weak SiO (5–4) and SiO (6–5): Sahai & Patel 2015). Hence, to our knowledge, the SiO emission we found in IRAS 16342$-$3814 is the highest velocity reported until now in pPNe. It is important to point out that previous studies show the SiO emission tracing the expanding CSE (see de Vicente et al. 2016, for a recent study of the SiO emission in evolved stars). Our data show SiO emission with higher velocities, by a factor of three, which must be tracing a different kinematic component, possibly related to the jet, given the similarity with the velocity spread of water masers. To our knowledge, only IRAS 16342$-$3814 presents EHV emission simultaneously in SiO, SO, HCN and ^{13}CO.

We assumed LTE conditions in order to calculate the column densities (N) of the molecular species found. In the case of SO, with the two transitions detected, we were able to provide an estimation of the rotational temperature and column density by employing a rotational diagram analysis (following Claude et al. 2000). In our calculations, we have applied beam-filling corrections to the line brightness temperatures, assuming a Gaussian source with a size of 0.5×2 arcsec^2 (e.g. Imai et al. 2012). We found T_{rot} in the range 5–11 K and N(SO) in the range 7.0×10^{16}–4.1×10^{18} cm^{-2}. For the other species we also assumed LTE, an excitation temperature of 11 K (i.e. the maximum T_{rot} we found for the narrow SO component) and the same source size for beam-filling corrections. The results are reported in Table 2.

Using the SO line ratio, we constrained the physical conditions of the extreme high-velocity gas. We have employed the offline version of RADEX (van der Tak et al. 2007) to generate a grid of line ratios, kinetic temperatures and H$_2$ volume densities. A more complete description of the RADEX calculations is provided in Supporting Information. We assume 2.73 K as the background temperature and a line width of 170 km s^{-1} (average FWHM of the two SO lines). We find that the SO line ratio is not very sensitive to column density within 10^{11} cm^{-2} to $\sim 10^{18}$ cm^{-2}. We point out that, with only one line ratio, it is only possible to provide lower limits to the kinetic temperature and volume density. The observed SO intensity ratio (from Table 1: $3988\pm453/1217\pm395 = 3.3\pm1.1$) constrains the lower limit of the H$_2$ volume density, $n_{\mathrm{H_2}} > 10^{4.8}$–$10^{5.7}$ cm^{-3}, and kinetic temperature, $T_{\mathrm{kin}} > 15$–55 K.

The H$_2$ mass of the SO extreme outflow is determined using the $n_{\mathrm{H_2}}$ lower limit estimated with the large velocity gradient (LVG) analysis from RADEX. Imai et al. (2012) modelled the CO emission and determined that the CSE/jet has a size in the range 6000–10 000 au. Assuming that the emission comes from a spheroid with

dimensions 6000 au $\times$ 6000 au $\times$ 10 000 au, which has a uniform $n_{\mathrm{H_2}}$ of $10^{4.8}$–$10^{5.7}$ cm^{-3} (best value of $10^{5.3}$ cm^{-3}), the mass of such a structure should be larger than $\sim$0.02–0.15 M$_\odot$ (0.06 M$_\odot$ for the best value). This mass estimate agrees very well with the mass calculated by Zijlstra et al. (2001, see their table 4), where the dust model of the innermost region gives a density of 10^8 cm^{-3}, a dust temperature of 80–200 K and a mass of 0.1 M$_\odot$. This lower limit to the mass is higher by up to a factor of five than the calculations for a fast outflow, as seen from the CO emission (see e.g. Sahai et al. 2006). Such dense, very fast and massive material may be related to a jet component. We point out, however, that the SO emission may come from a smaller (shocked) region than the one traced by CO, which then would increase the $n_{\mathrm{H_2}}$ estimation. Interferometric mm-wavelength observations with angular resolution below 1 arcsec are needed to probe the structure of the SO EHV emission in greater detail.

In order to test the effect of magnetic fields, we provide a rough estimate of the field intensity needed to broaden the SO line to a few hundred km s^{-1}, assuming the Zeeman effect exclusively. Using the formulae given in Bel & Leroy (1989), we calculated that the minimum field detectable is of the order of mG. For a broadening of $\sim$60–90 MHz, the magnetic field intensity needed is $\sim$70 G. Vlemmings (2014) estimated $\sim$100 G for the upper limit for the magnetic field near the stellar surface for AGB stars, so our estimations are consistent with this limit. However, the resolution of the RSR prevents us from saying anything more conclusive.

4.2 Molecular abundances in EHV gas

In Table 2, we report the molecular abundances (X) computed using the column-density estimations and the expression $X = X(^{13}\mathrm{CO}) \times N/N(^{13}\mathrm{CO})$, where $X(^{13}\mathrm{CO})$ is assumed to be 2×10^{-5} (following Bujarrabal et al. 2001). We notice that the SO abundance (4.0×10^{-7}) is consistent with results of the SO wings in OH 231.8+4.2 Claude et al. (2000). The abundance of SiO (5.2×10^{-7}) is lower by two orders of magnitude than in IRAS 08005$-$2356, the other known SiO extreme outflow (Sahai & Patel 2015). The HCN abundance (9.6×10^{-8}) is more similar to the lower limit calculated in CRL 618 for low-velocity HCN emission ($>2 \times 10^{-7}$) than for high-velocity (4×10^{-6}) (Sánchez Contreras & Sahai 2004).

The SiO/HCN abundance ratio is $\sim$5, suggesting that C-bearing molecules are depleted in the extreme outflow. In contrast, in the other O-rich pPN with an extreme outflow, OH 231.8+4.2, such an abundance ratio is $\sim$0.5 for the EHV range (average of $\sim$0.3 for the whole line emission range: Sanchez Contreras et al. 1997). On the other hand, the SiO/SO abundance ratio is close to one, which therefore implies that the elemental abundances of Si and S are similar, in sharp contrast with OH 231.8+4.2, for which such a ratio is $\sim 10^{-2}$ (Sanchez Contreras et al. 1997; Claude et al. 2000). A remarkable result is that the highest abundances are those of SiO and SO, which suggests that the extreme high-velocity gas is dominated by O-bearing molecules. It is well known that the extreme outflow in OH 231.8+4.2 is more prominent in HCN than in SiO (e.g. Sanchez Contreras et al. 1997), which may indicate that this kinematic component, in contrast to IRAS 16342$-$3814, is more C-rich than O-rich. In that respect, it is relevant to notice that the O-rich EHV gas in the pPN presented here is more similar to what is found in the star-formation case (Tafalla et al. 2010).

Despite the abundance trend differences noted with respect to OH 231.8+4.2, there is still the similarity that both pPNe present a very fast outflow. It has been suggested that shocks from the extreme outflow of OH 231.8+4.2 may have a major impact on the

rich chemistry observed in that source. Velilla Prieto et al. (2015), for example, discuss the possibility of molecular reformation after high-speed shocks, through the interaction of the jet and the CSE, destroy the molecules. They propose, in particular, that additional atoms (such as Si and S) may be released to the gas phase from dust grains by the actions of the shocks and, when the shocked material has cooled down sufficiently to allow molecular reformation, there is a different proportion of the elements available for reactions in the post-shocked gas, affecting the abundances of a second generation of molecules. Such a process may also be applicable to the case of IRAS 16342−3814. In that regard, we notice that the SiO abundance is close to the range predicted by shock chemistry models (SiO production in the gas phase through the sputtering of Si-bearing material in refractory grain cores: Gusdorf et al. 2008), which may give support to such a scenario. However, we point out that the caveat here is that the abundance calculations are dependent on the assumed value of the excitation temperature (which can be different for different molecules), hence a better estimation of such a quantity is required before drawing any general conclusion. Also, the limitation of our spectral line data is that it is difficult to separate the contribution from low-velocity (circumstellar envelope) and high-velocity (jet) components. Hence the abundances reported here are the average of both components, which may not be sufficient for detailed future shock-chemistry models.

5 CONCLUSIONS

(i) Our modest 1.5-h LMT observations with the RSR proved to be a good strategy to test the chemical content of extreme velocity outflows from pPNe.

(ii) With a line width of $\sim$240 km s^{-1}, we found the highest velocity SO outflow in a pPN.

(iii) The HCN emission has a velocity spread similar to CRL618, the other pPN known with high-velocity HCN.

(iv) We found the highest velocity SiO emission in a pPN, which may trace a different kinematic component with respect to previous SiO observations in evolved stars, possibly related to a jet.

(v) By using a SO line ratio, we found that the extreme outflow consists of dense gas ($n_{H_2} > 10^{4.8}$–$10^{5.7}$ cm^{-3}), with a mass of $\sim$0.02–0.15 M$_\odot$.

(vi) We found a weak indication of very fast SO (3$_2$–2$_1$) emission reaching velocities ~ -700 km s^{-1}, which, if confirmed, would be the fastest molecular outflow ever found in a protoplanetary nebula.

ACKNOWLEDGEMENTS

NOTE ADDED IN PROOF

In a recent paper, Sahai et al. (2017) report extremely high velocity emission, up to relative velocities of $\pm$260 km s^{-1}, in the CO (3−2) and H^{13}CN (4−3) lines.

REFERENCES

Bachiller R., 1996, ARA&A, 34, 111
Balick B., Huarte-Espinosa M., Frank A., Gomez T., Alcolea J., Corradi R. L. M., Vinković D., 2013, ApJ, 772, 20
Bel N., Leroy B., 1989, A&A, 224, 206
Bujarrabal V., Castro-Carrizo A., Alcolea J., Sánchez Contreras C., 2001, A&A, 377, 868
Chong S.-N., Imai H., Diamond P. J., 2015, ApJ, 805, 53
Claude S. M. X., Avery L. W., Matthews H. E., 2000, ApJ, 545, 379
Claussen M. J., Sahai R., Morris M. R., 2009, ApJ, 691, 219
Cybulski R. et al., 2016, MNRAS, 459, 3287
de Vicente P. et al., 2016, A&A, 589, A74
Erickson N., Narayanan G., Goeller R., Grosslein R., 2007, in Baker A. J., Glenn J., Harris A. I., Mangum J. G., Yun M. S., eds, ASP Conf. Ser. Vol. 375, From Z-Machines to ALMA: (Sub)Millimeter Spectroscopy of Galaxies. Astron. Soc. Pac., San Francisco, p. 71
Gómez J. F., Rizzo J. R., Suárez O., Miranda L. F., Guerrero M. A., Ramos-Larios G., 2011, ApJ, 739, L14
Gusdorf A., Cabrit S., Flower D. R., Pineau Des Forêts G., 2008, A&A, 482, 809
He J. H., Imai H., Hasegawa T. I., Campbell S. W., Nakashima J., 2008, A&A, 488, L21
Imai H., He J.-H., Nakashima Nobuharu J.-I. U., Deguchi S., Koning N., 2009, PASJ, 61, 1365
Imai H., Chong S. N., He J.-H., Nakashima J.-i., Hsia C.-H., Sakai T., Deguchi S., Koning N., 2012, PASJ, 64
Lefloch B. et al., 2015, A&A, 581, A4
Sahai R., Patel N. A., 2015, ApJ, 810, L8
Sahai R., Trauger J. T., 1998, AJ, 116, 1357
Sahai R., te Lintel Hekkert P., Morris M., Zijlstra A., Likkel L., 1999, ApJ, 514, L115
Sahai R., Young K., Patel N. A., Sánchez Contreras C., Morris M., 2006, ApJ, 653, 1241
Sahai R., Vlemmings W. H. T., Gledhill T., Sanchez Contreras C., Lagadec E., Nyman L.-A., Quintana-Lacaci G., 2017, ApJ, 835, L13
Sánchez Contreras C., Sahai R., 2004, ApJ, 602, 960
Sanchez Contreras C., Bujarrabal V., Alcolea J., 1997, A&A, 327, 689
Tafalla M., Santiago-García J., Hacar A., Bachiller R., 2010, A&A, 522, A91
van der Tak F. F. S., Black J. H., Schöier F. L., Jansen D. J., van Dishoeck E. F., 2007, A&A, 468, 627
Velilla Prieto L. et al., 2015, A&A, 575, A84
Vlemmings W. H. T., 2014, in Petit P., Jardine M., Spruit H. C., eds, IAU Symp. Vol. 302, Magnetic Fields throughout Stellar Evolution. Cambridge Univ. Press, Cambridge, p. 389, doi: 10.1017/S1743921314002580
Yung B. H. K., Nakashima J.-i., Hsia C.-H., Imai H., 2016, MNRAS, 465, 4482
Zijlstra A. A., Chapman J. M., te Lintel Hekkert P., Likkel L., Comeron F., Norris R. P., Molster F. J., Cohen R. J., 2001, MNRAS, 322, 280

SUPPORTING INFORMATION

Supplementary data are available at *MNRASL* online.

Appendix A

Please note: Oxford University Press is not responsible for the content or functionality of any supporting materials supplied by the authors. Any queries (other than missing material) should be directed to the corresponding author for the article.

This paper has been typeset from a TₑX/LᴬTₑX file prepared by the author.